
















Detection of the Polycyclic Aromatic Hydrocarbon Phenalene (C₁₃H₁₀) in the Very Low Luminosity Object (VeLLO) MC27/L1521F

GABI WENZEL ^{1,2} THOMAS H. SPEAK ³ CI XUE ^{4,5} EDWIN A. BERGIN ⁶ ANDREW M. BURKHARDT ⁷
MARTIN A. CORDINER ⁸ MIYA DUFFY ¹ ZACHARY T. P. FRIED ¹ ANDREW LIPNICKY ⁴
CHRISTOPHER N. SHINGLEDECKER ⁹ REACE H. J. WILLIS ³ ANTHONY J. REMIJAN ⁴ MICHAEL C. MCCARTHY ²
BRETT A. MCGUIRE ^{1,4} AND ILSA R. COOKE ³

¹*Department of Chemistry, Massachusetts Institute of Technology, Cambridge, MA 02139, USA*

²*Center for Astrophysics | Harvard & Smithsonian, Cambridge, MA 02138, USA*

³*Department of Chemistry, University of British Columbia, Vancouver, BC V6T 1Z1, Canada*

⁴*National Radio Astronomy Observatory, Charlottesville, VA 22903, USA*

⁵*NSF-Simons AI Institute for Cosmic Origins, Austin, TX, 78712, USA*

⁶*Department of Astronomy, University of Michigan, Ann Arbor, MI 48109, USA*

⁷*Department of Earth, Environment, and Physics, Worcester State University, Worcester, MA 01602, USA*

⁸*Astrochemistry Laboratory and the Goddard Center of Astrobiology, Solar System Exploration Division, NASA Goddard Space Flight Center, Greenbelt, MD 20771, USA*

⁹*Department of Chemistry, Virginia Military Institute, Lexington, VA 24450, USA*

ABSTRACT

To date, 14 polycyclic aromatic hydrocarbons (PAHs) ranging in size from two to seven (including five- and six-membered) carbon rings have been detected in the starless dense core TMC-1 CP within the Taurus molecular cloud. Their detection raises questions about the distribution of PAHs in the cold interstellar medium (ISM) and their evolution during star formation. Here, we present the first interstellar detection of a three-ring PAH outside of TMC-1 CP. We detect phenalene (C₁₃H₁₀), a compact, peri-fused PAH, in the dense core MC27/L1521F, a molecular cloud in Taurus containing a very low-luminosity object (VeLLO). We compare the abundances of phenalene in the two sources with respect to the single-ring aromatic benzonitrile, and find that it is enhanced by a factor of four in MC27/L1521F. We discuss the implications for possible formation and destruction pathways in the two sources. These findings further support the widespread abundance of PAHs throughout the cold ISM and are consistent with survival, inheritance, or replenishment during the earliest stages of star formation.

Keywords: Astrochemistry (75); Polycyclic aromatic hydrocarbons (1280); Interstellar medium (847); Interstellar molecules (849); Radio astronomy (1338); Surveys (1671)

1. INTRODUCTION

Polycyclic aromatic hydrocarbons (PAHs) are key components of the interstellar medium (ISM) and have been established as major carbon reservoirs. While their interstellar presence has been assumed since the 1980s (A. Léger & J. L. Puget 1984; L. J. Allamandola et al. 1985), unambiguous evidence was delivered recently with the detections of cyano-functionalized PAHs (CN-PAHs) in the dark and cold Taurus molecular cloud (TMC-1) ranging from two to up to seven perifused

aromatic rings, namely naphthalene, acenaphthylene, pyrene, and coronene (B. A. McGuire et al. 2021; J. Cernicharo et al. 2024, 2026; G. Wenzel et al. 2024, 2025a,b). These results stem from two sensitive line surveys using single dish radio telescopes; the Green Bank Telescope (GBT) Observations of TMC-1: Hunting for Aromatic Molecules (GOTHAM; B. A. McGuire et al. 2020) and Q-band Ultrasensitive Inspection Journey to the Obscure TMC-1 Environment (QUIJOTE; J. Cernicharo et al. 2021b) projects.

Depending on their symmetry and substitution pattern, bare or unsubstituted PAHs possess small to zero permanent electric dipole moments, making the CN-PAHs attractive proxies with bright rotational transi-

tions (B. A. McGuire et al. 2018; I. R. Cooke et al. 2020; M. C. McCarthy & B. A. McGuire 2026). Nevertheless, the bare PAHs 1H-indene, 1H-cyclopent[cd]indene, and 1H-phenalene, with permanent electric dipole moments of approximately 0.5–0.8 D, have been detected in TMC-1 CP (Cyanopolyne Peak) thanks to their radio emission and large abundance (A. M. Burkhardt et al. 2021b; J. Cernicharo et al. 2021a; R. Fuentetaja et al. 2026; C. Cabezas et al. 2025). The substantial extent of the carbon reservoir held by PAHs in TMC-1 CP was rather unexpected, as was the flat abundance distribution irrespective of size or molecular complexity (G. Wenzel et al. 2025b; V. M. Rivilla et al. 2026; M. Agúndez & J. Cernicharo 2026), defying the near universal trend of decreasing abundance with increasing size within a molecular “family” (R. A. Loomis et al. 2016, 2021).

TMC-1 CP is a starless core before protostar formation, but not the only source hosting aromatic molecules. The single-ring aromatic molecule benzonitrile has been identified toward sources located in Taurus, Serpens, Lupus, and Aquila (A. M. Burkhardt et al. 2021a; M. Agúndez et al. 2023) and most recently in the Central Molecular Zone (V. M. Rivilla et al. 2026). Additionally, the two-ring molecule 1H-indene was detected toward the quiescent starless core L1495B (M. Agúndez et al. 2023), a source in Taurus exhibiting increased abundances of oxygen-bearing sulfur species when compared to other starless or prestellar cores (L. Schöller et al. 2026). A representative object transitioning from the prestellar core stage to the protostar phases has been observed toward MC27/L1521F (C. Favre et al. 2020). This source hosts a very-low-luminosity object (VeLLO) — objects with a luminosity of $L_{\text{int}} < 0.1L_{\odot}$ associated with dense cores (J. Kauffmann et al. 2005) — where the embedded protostar is just beginning to heat up (T. L. Bourke et al. 2006). A. M. Burkhardt et al. (2021a) detected the single-ring benzonitrile in MC27/L1521F, indicating its survival during the onset of star formation.

The three-ring PAH 1H-phenalene ($C_{13}H_{10}$), hereafter phenalene, has been previously detected in TMC-1 CP (C. Cabezas et al. 2025). Phenalene consists of a naphthalene subunit, with an ortho- and peri-fused cyclohexene ring (see Figure 1). An H atom from the CH_2 group in phenalene can be readily removed to form a resonantly stabilized radical, phenalenyl. Its relevance to combustion chemistry motivated the first gas-phase laboratory detection of phenalenyl (G. D. O’Connor et al. 2011), and it has since been speculated to play an important role in PAH growth in flames (K. O. Johansson et al. 2018).

Here, we report the detection of phenalene toward MC27/L1521F in high abundance, the first three-ring PAH detected outside of TMC-1 CP.

2. OBSERVATIONS

All observations were acquired on the 100 m Robert C. Byrd Green Bank Telescope (GBT) as part of two large, ongoing spectral line surveys: GBT Observations of TMC-1: Hunting for Aromatic Molecules (GOTHAM; B. A. McGuire et al. 2020) and A Rigorous K/Ka -Band Hunt for Aromatic Molecules (ARKHAM; A. M. Burkhardt et al. 2021a). Details of the observing strategies and data reduction procedures were previously described by C. Xue et al. (2025), including advances in artifact and radio-frequency interference removal, atmospheric opacity corrections, and baseline removal.

Briefly, the GOTHAM survey targets the “Cyanopolyne Peak” of TMC-1 centered at $\alpha_{J2000} = 04^{\text{h}}41^{\text{m}}42.5^{\text{s}}$, $\delta_{J2000} = +25^{\circ}41'26.8''$ and spans 29 GHz of bandwidth between 4–36 GHz at a spectral resolution of 1.4 kHz. The root-mean-squared (RMS) noise level ranges between 3.8–15.0 mK across the majority of the observed frequency range. Flux calibration was carried out using switched noise-diode measurements, yielding an estimated antenna temperature accuracy of 10–20%. The GOTHAM observations cover the C -, X -, Ku -, K - and Ka -bands. The ARKHAM survey was designed to target multiple sources for benzonitrile detection. In particular, MC27/L1521F was observed centering the GBT at $\alpha_{J2000} = 04^{\text{h}}28^{\text{m}}39.3^{\text{s}}$, $\delta_{J2000} = +26^{\circ}51'39.0''$ covering a frequency range of 22–30.5 GHz of the K - and Ka -bands. The ARKHAM data were recalibrated using the newly developed GOTHAM Spectral Pipeline (C. Xue et al. 2025) to properly correct for zenith opacity, particularly around the 22 GHz water vapor line, and to better constrain the noise properties by reducing the noise covariance. The RMS noise level ranges between 5.2–23.5 mK across the majority of the observed frequency range.

3. ASTRONOMICAL ANALYSIS

The laboratory rotational spectrum of phenalene was measured and fit by C. Cabezas et al. (2025) and its spectroscopic constants, partition function, and spectral line catalog are publicly available in the Cologne Database for Molecular Spectroscopy (CDMS)¹⁰ (C. P. Endres et al. 2016). Together with its laboratory analysis, C. Cabezas et al. (2025) also reported the first interstellar detection of phenalene in the QUIJOTE ob-

¹⁰ <https://cdms.astro.uni-koeln.de/classic/>

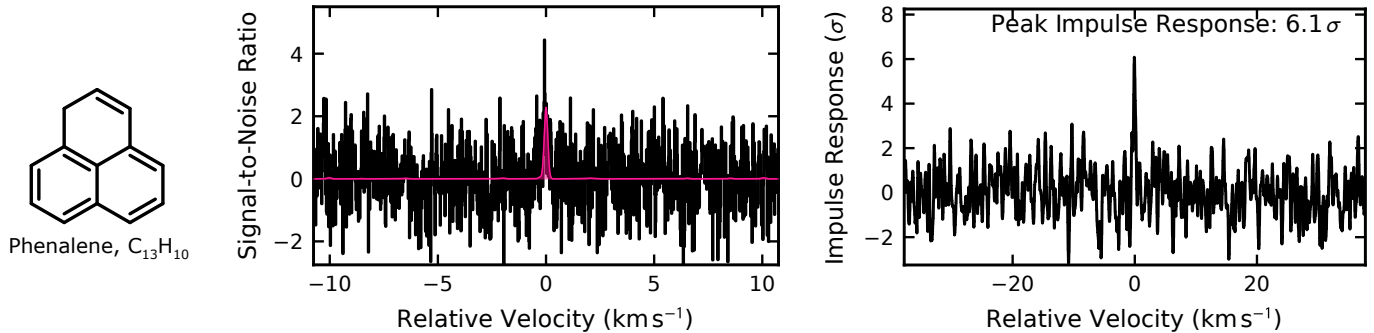


Figure 1. (Left) Structure of 1H-phenalene (C₁₃H₁₀). (Center) Velocity-stacked spectra and (right) matched filter response of phenalene emission in the ARKHAM data toward MC27/L1521F generated using the methodologies outlined in R. A. Loomis et al. (2021).

servations conducted with the 40 m Yebes radio telescope toward TMC-1 CP. Simulating the radio emission of phenalene under TMC-1 CP conditions (see Tables A1 and A2) and performing a velocity-stack and matched filter response analysis (R. A. Loomis et al. 2021), we also detect this molecule in the fifth data reduction (DRV) of the GOTHAM dataset (C. Xue et al. 2025) from the GBT with a significance of 18.2σ (see Figure A1). Using the Markov Chain Monte Carlo (MCMC) analysis adopted from previous work (B. A. McGuire et al. 2021; R. A. Loomis et al. 2021), we derive an excitation temperature of $9.91^{+1.73}_{-1.33}$ K and a column density of $1.53^{+0.27}_{-0.14} \times 10^{13} \text{ cm}^{-2}$ that best describe the emission from phenalene in TMC-1 CP. This is in agreement with the previously reported temperature of (7.9 ± 1.2) K and column density of $(2.8 \pm 1.6) \times 10^{13} \text{ cm}^{-2}$ by C. Cabezas et al. (2025).

The search for phenalene toward MC27/L1521F was performed analogously. We first simulated the rotational spectrum of benzonitrile under the physical conditions present in MC27/L1521F and performed an MCMC analysis on the newly reduced ARKHAM data informed by the previous detection of benzonitrile in this source (A. M. Burkhardt et al. 2021a). The results are listed in Table A3 and agree with the previous analysis. We performed an MCMC analysis using priors constrained by our benzonitrile detection in MC27/L1521F to derive physical parameters that best describe the emission of phenalene (see Tables A1 and A3). Using these values, we simulated the phenalene emission in MC27/L1521F and carried out a velocity-stack and matched filter analysis (see Figure 1) of the ARKHAM data (A. M. Burkhardt et al. 2021a). We derive a detection significance of phenalene toward MC27/L1521F of 6.1σ . At the RMS noise level of the observations of 5.2–23.5 mK, individual emission lines of phenalene are not detected above the noise. From the MCMC analysis, we derive an excitation temperature of $4.91^{+0.08}_{-0.08}$ K and a column density of $1.47^{+0.49}_{-0.35} \times 10^{13} \text{ cm}^{-2}$, which

is similar to the column density of phenalene found in TMC-1 CP.

The ratio of phenalene-to-benzonitrile, however, differs significantly between both sources. The phenalene/benzonitrile ratio in TMC-1 CP is ~ 9 ($9.27^{+1.71}_{-0.91}$), whereas this ratio is ~ 40 ($40.2^{+14.7}_{-11.5}$) in MC27/L1521F, making phenalene a factor of ~ 4 more abundant in MC27/L1521F when comparing to benzonitrile than in TMC-1 CP. Figure 2 compiles the abundances of interstellar (P)AHs with respect to molecular hydrogen (values listed in Table B4) as a function of molecular complexity, starting with the single-ring benzonitrile. While generally the bare (unsubstituted) PAHs in TMC-1 CP are approximately one order of magnitude more abundant than CN-(P)AHs, this ratio is clearly changed in MC27/L1521F.

4. DISCUSSION

To date, the formation pathways of most PAHs found at the earliest stages of star formation, in sources such as TMC-1 or MC27/L1521F, are predominantly unknown. One of the major known formation routes of PAHs is the H-abstraction acetylene (C₂H₂) addition (HACA) mechanism that involves substantial reaction barriers (M. Frenklach et al. 1985; E. Reizer et al. 2022). Such barriers cannot be surmounted in cold cores, but can be overcome in high-temperature environments such as those found in flames or combustion processes or in carbon-rich circumstellar environments (M. Frenklach et al. 2024). In such environments, the production of the phenalenyl radical has been studied through a reaction scheme of acenaphthylene and methane in an electrical discharge (Z. D. Levey et al. 2022). This was supported by prior theoretical work that characterized a barrierless formation route to the phenalenyl radical via phenalene in the reaction of 1-acenaphthyl and methyl radicals (D. P. Porfiriev et al. 2020). If occurring in tandem with, e.g., HACA, this process might produce larger PAHs in flames and the ISM. L. Zhao et al. (2020) proposed an-

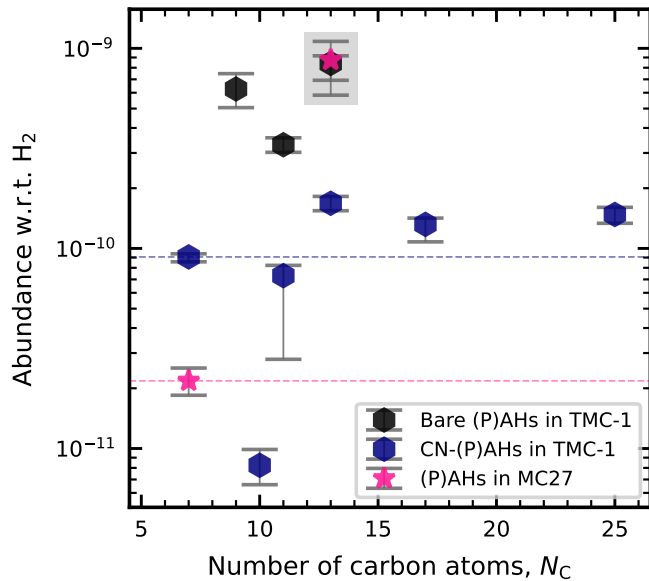


Figure 2. Abundance of detected (polycyclic) aromatic hydrocarbons ((P)AHs) in TMC-1 CP (blue and black hexagons) and in MC27/L1521F (magenta stars) with respect to the molecular hydrogen abundance in each source and as a function of number of carbon atoms per molecule, N_C . Dashed horizontal lines are the propagated benzonitrile abundances to guide the eye. The area shaded in grey highlights the high abundance of phenalene in TMC-1 and MC27/L1521F. Column density values and the references they originate from are reported in Table B4.

other gas-phase formation route to phenalene via the reaction of the 1-naphthyl radical with methylacetylene and allene under high-temperature conditions, which likewise could occur in circumstellar environments.

MC27/L1521F is a source hosting a newly formed Class 0 protostar (K. Tokuda et al. 2026) producing ultraviolet (UV) radiation. VeLLOs are thought to undergo episodic accretion episodes, in which the accretion rate may be substantially enhanced relative to their present quiescent state. As the far-UV (FUV) field scales with accretion rate (H. Yang et al. 2011), MC27/L1521F may have experienced periods with a significantly enhanced FUV field relative to both the standard interstellar radiation field, as well as TMC-1 CP. For accretion rates on the order of $10^{-8} M_{\odot} \text{ yr}^{-1}$, local radiation fields of $G_0 \sim 10^2 - 10^3$ are plausible at radii of ~ 100 AU (E. Bergin et al. 2003).

The enhanced phenalene/benzonitrile ratio in MC27/L1521F may reflect differing photostabilities of the two species. With a more intense UV radiation field present in MC27/L1521F, photodissociation of benzonitrile could be more efficient (see, for example, J. Kamer et al. (2023); D. B. Rap et al. (2024); D. B. Debes et al. (2025)) compared to that of phenalene, and thus

enhance the phenalene/benzonitrile ratio. However, absolute interstellar photodissociation rates for the neutral species have not been reported, making quantitative comparisons difficult. The exceptionally weak C-H bonds in the CH_2 moiety of phenalene ($258.1 \text{ kJ mol}^{-1}$; G. D. O’Connor et al. 2017) likely lowers its dissociation thresholds compared to fully aromatic PAHs, which may enhance fragmentation (D. P. Porfiriev et al. 2020; A. Marciniak et al. 2021). Conversely, phenalene possesses a higher density of states than benzonitrile, which may enhance internal energy redistribution and cooling, resulting in a longer lifetime prior to fragmentation. In addition, phenalene has a larger number of vibrational modes from which infrared emission can occur. The combination of these factors would tend to favor stabilization of phenalene as compared to benzonitrile.

Recent work has shown that recurrent fluorescence (RF) offers an efficient route for radiatively cooling PAH cations, quenching dissociation and leading to their enhanced stability upon UV excitation (M. H. Stockett et al. 2023; A. Subramani et al. 2025; J. N. Bull et al. 2025). Although RF rates for the phenalene cation have not yet been measured, its larger vibrational manifold may favor more efficient radiative stabilization compared to the benzonitrile cation. The relative stability of phenalene and benzonitrile under interstellar UV irradiation depends sensitively on the competition between fragmentation and radiative stabilization.

The abundance (with respect to H_2) that we derive for benzonitrile in MC27/L1521F is roughly five times lower than that in TMC-1 CP, $\sim 2 \times 10^{-11}$ versus $\sim 9 \times 10^{-11}$, respectively. In contrast, the phenalene abundance in the two sources is similar, $\sim 10^{-9}$. However, it is important to note that there is considerable uncertainty on the H_2 column density reported for MC27/L1521F. The H_2 column density may be higher within the primary beam of the GBT than the weighted mean value originally derived by S. Chitsazzadeh (2014), resulting in lower abundances of both benzonitrile and phenalene.

Benzonitrile has now been observed in a number of cold molecular cloud sources in Lupus, Taurus, Aquila, and Serpens (B. A. McGuire et al. 2018; A. M. Burkhardt et al. 2021a; M. Agúndez et al. 2023), as well as recently in warmer gas in the Central Molecular Zone (V. M. Rivilla et al. 2026). The sources containing protostars, L1527 in Taurus and L483 in Aquila, have the lowest benzonitrile abundances. Variations in the abundances across the sources may reflect differences in the physical conditions, such as the local FUV fields, or chemical evolution effects, such as differences in the partitioning of carbon and oxygen between the gas and dust. MC27/L1521F is a more dy-

namically evolved and denser core than TMC-1 CP, exhibiting strong CO freezeout (A. Crapsi et al. 2004); therefore, H_3^+ and N_2H^+ (which are predominantly destroyed through reactions with gas-phase CO) will likely be more abundant. Such differences in key molecular ions may cause downstream chemical effects on the carbon reservoirs, resulting in differences in the phenalene/benzonitrile abundance ratios.

Lastly, phenalene has been noted to potentially form pyrene (M. Frenklach et al. 2024), another interstellar PAH that has been found in TMC-1 CP via its CN-derivatives (G. Wenzel et al. 2024, 2025a). So far, the synthesis route of pyrene in the cold ISM is not understood; however, L. Zhao et al. (2018) showed its formation via a HACA mechanism from phenanthrenyl in the high-temperature environments of carbon-rich circumstellar envelopes. Detecting the three-ring PAH, phenalene, in the cold cloud MC27/L1521F shows the critical importance of understanding interstellar PAH chemistry, as these large carbon reservoirs will be directly available to star and planet formation.

The unsubstituted phenalene is another candidate to test the so-called “proxy method”, in which column densities of some “bare” PAHs have been inferred through the detection of cyano-substituted PAHs with large permanent electric dipole moments. To date, only one bare aromatic molecule and one of its cyano-functionalized derivatives have both been detected in the same source, namely indene and 2-cyanoindene in TMC-1 CP (A. M. Burkhardt et al. 2021b; J. Cernicharo et al. 2021a; M. L. Sita et al. 2022; C. Xue et al. 2025), with a ratio of parent-to-child of $\text{H}/\text{CN} = 76_{-36}^{+49}$ based on the column densities in C. Xue et al. (2025). The detection of the untagged parent phenalene presents another potential opportunity to better constrain the proxy method. As such, we carried out preliminary work (see Appendix C) that verifies CN addition followed by H atom elimination at sites 2–9 of phenalene occurs over deeply submerged barriers. Combining this with overall rate coefficients estimated using classical capture theory rate coefficients and the modeled rate dependence of CN tagged child-to-bare-parent-PAH determined in G. Wenzel et al. (2025a) and used in G. Wenzel et al. (2025b) yields $2.18_{-1.19}^{+2.96} \times 10^{12}$, cm^{-2} , with the expected isomer specific abundance being $2.72_{-1.49}^{+3.70} \times 10^{11}$ cm^{-2} , suggesting that 1-cyano-1H-phenalene could be formed with an abundance up to $9.07_{-4.98}^{+12.34} \times 10^{11}$ cm^{-2} . However, a dedicated interstellar search for the cyanophenalenes will require their rotational spectra to be first characterized in the laboratory.

5. CONCLUSIONS

We report the detection of a three-ring PAH outside of TMC-1 CP. Phenalene ($\text{C}_{13}\text{H}_{10}$) was identified using legacy ARKHAM data (A. M. Burkhardt et al. 2021a) toward the dense molecular cloud core MC27/L1521F with a column density of $1.47_{-0.35}^{+0.49} \times 10^{13}$ cm^{-2} at an excitation temperature of $4.91_{-0.08}^{+0.08}$ K. The phenalene/benzonitrile ratio is four times larger in MC27/L1521F than the one derived for TMC-1 CP. So far, no low-temperature formation pathways to phenalene that could occur under cold cloud conditions are known. This motivates further studies of UV-driven PAH chemistry under interstellar conditions. Nevertheless, this detection signifies the prevalence of PAHs across the cold ISM, where they are carbon reservoirs available during protostar formation.

6. DATA ACCESS & CODE

The raw data of the GOTHAM observations are publicly available from C. Xue et al. (2025) and in the GBT Legacy Data Archive¹¹. The ARKHAM data is available in A. M. Burkhardt et al. (2021a). The GOTHAM Spectral Pipeline¹² used for the astronomical data reduction is publicly available in C. Xue (2025) and the analysis was carried out using the mol_{sim}¹³ open-source software package; an archival version of the code can be accessed at B. A. McGuire et al. (2024).

ACKNOWLEDGEMENTS

We gratefully acknowledge support from NSF grants AST-1908576, AST-2205126, and AST-2307137. G.W. and B.A.M. acknowledge the support of the Arnold and Mabel Beckman Foundation Beckman Young Investigator Award. G.W. and B.A.M. also gratefully acknowledge the support of Schmidt Family Futures. I.R.C. acknowledges support from the University of British Columbia and the Natural Sciences and Engineering Research Council of Canada (RGPIN-2022-04684). I.R.C. and T.H.S. acknowledge the support of the Canadian Space Agency through grant 24AO3UBC14 and this work was in part supported through the computational resources and services provided by Advanced Research Computing at the University of British Columbia. C.X. acknowledges support from the National Science Foundation under Cooperative Agreement 2421782 and the Simons Foundation grant MPS-AI-00010515 awarded to

¹¹ <https://greenbankobservatory.org/portal/gbt/gbt-legacy-archive/gotham-data/>

¹² <https://github.com/cixue/gotham-spectral-pipeline>

¹³ <https://github.com/bmcguir2/mol_{sim}>

the NSF-Simons AI Institute for Cosmic Origins – CosmicAI, <https://www.cosmicai.org/>. The National Radio Astronomy Observatory is a facility of the National Science Foundation operated under cooperative agreement by Associated Universities, Inc. The Green Bank Observatory is a facility of the National Science Foundation operated under cooperative agreement by Associated Universities, Inc.

AUTHOR CONTRIBUTIONS

G.W.: Conceptualization, Data Curation, Formal analysis, Investigation, Visualization, Writing – original draft. T.H.S.: Data Curation, Investigation, Resources, Writing – original draft. C.X.: Data Curation, Invest-

igation, Software, Validation. E.A.B., A.M.B, M.A.C, M.D., Z.T.P.F, A.L., C.N.S., R.H.J.W.: Investigation. A.J.R.: Resources, Supervision. M.C.M.: Funding acquisition, Resources, Supervision. B.A.M.: Funding acquisition, Methodology, Resources, Supervision. I.R.C.: Funding acquisition, Investigation, Resources, Supervision, Writing – original draft. All authors contributed to Writing – review & editing and are members of the GOTHAM collaboration.

Facility: GBT

Software: GOTHAM Spectral Pipeline (C. Xue et al. 2025), molsim (B. A. McGuire et al. 2024)

APPENDIX

A. MCMC ANALYSES OF PHENALENE IN TMC-1 AND MC27/L1521F

MCMC analyses were performed analogously to the methodologies outlined by R. A. Loomis et al. (2021) and priors were informed by previous works of the GOTHAM team and benzonitrile detections from the ARKHAM project, see in particular C. Xue et al. (2025) and A. M. Burkhardt et al. (2021a). The priors used in this work for MCMC analyses of molecular emission in TMC-1 CP and MC27/L1521F are listed in Table A1 and the results are reported in Tables A2 and A3 for molecular emission in TMC-1 CP and MC27/L1521F, respectively. Figure A1 demonstrates the velocity-stack and matched filter analysis of phenalene in TMC-1 CP (upper panels) and benzonitrile in MC27/L1521F (lower panels). Note that the weak signal observed at non-zero relative velocities in the benzonitrile velocity-stack is from benzonitrile. Due to ^{14}N nuclear quadrupole hyperfine splitting, benzonitrile contains many closely spaced lines that will be contained in the extracted spectral windows centered on each line. The posteriors of the benzonitrile detection in MC27/L1521F were used to inform the priors used for the phenalene analysis in the same source. Figures A2 and A3 depict the covariance plots of each detection.

B. COLUMN DENSITIES OF CYCLIC AROMATIC HYDROCARBONS IN TMC-1 CP AND MC27/L1521F

The data compiled in Fig. 2 is listed in Table B4. The references these values originate from are given.

C. AB-INITIO CHARACTERIZATION OF THE REACTION OF CN AND PHENALENE

C.1. *Potential energy surface calculations*

An ab-initio potential energy surface for the reaction of CN and phenalene was calculated. Initial geometries for the reactants, products and adducts were produced in Avogadro (M. D. Hanwell et al. 2012). Optimizations and harmonic frequency analyses were performed with the density functional theory (DFT) ωB97M (J.-D. Chai & M. Head-Gordon 2008; N. Mardirossian & M. Head-Gordon 2016; S. Lehtola et al. 2018) hybrid functional and the D4 empirical dispersion correction (E. Caldeweyher et al. 2019, 2020), along with the minimally augmented triple zeta Karlsruhe basis set ma-def2-TZVPP (F. Weigend & R. Ahlrichs 2005; J. Zheng et al. 2011; F. Weigend 2006) with very tight convergence criteria for both SCF and optimizations and the DEFGRID3 integration grid. Harmonic zero point energies were scaled for anharmonicity by 0.9779 (M. K. Kesharwani et al. 2014). Initial geometries for transition states were obtained from relaxed (all but scan coordinate minimized) scans of the forming or breaking of bonds. Following optimization, transition states were evaluated for the presence of a single imaginary mode, and intrinsic reaction coordinate scans (IRCs) (K. Ishida et al. 1977; F. Neese et al. 2020) verified they linked products and reactants. Single point energies for $\omega\text{B97M-D4/ma-def2-TZVPP}$ stationary points were refined using explicitly correlated couple cluster with singles and doubles and perturbative triple excitations CCSD(T)-F12c (T. B. Adler et al. 2007; G. Knizia et al. 2009; G. Rauhut et al. 2009) including a resolution of integral (RI) approximation on the F12 component (E. F. Valeev 2004; J. Noga & J. Simunek 2009;

Table A1. Priors used for the MCMC analysis. A Gaussian distribution, $\mathcal{N}(\mu, \sigma^2)$, with mean μ and variance σ^2 , was used for velocity, v_{LSR} , both in TMC-1 and in MC27/L1521F. For TMC-1, a uniform (unweighted) distribution, $\mathcal{U}\{\text{min, max}\}$, between min and max was used for the source size, column density, N_{T} , excitation temperature, T_{ex} , and linewidth, ΔV . Due to phenalene’s faint emission in MC27/L1521F, priors were more constrained with a fixed source size, $\delta(x)$, and Gaussian distributions for excitation temperature, T_{ex} , and linewidth, ΔV . The column density was varied using a uniform (unweighted) distribution, $\mathcal{U}\{\text{min, max}\}$. Priors were adopted from our previous comprehensive analysis of aromatic molecules in TMC-1 **using four velocity components** (C. Xue et al. 2025) and benzonitrile in MC27/L1521F **using two velocity components** (A. M. Burkhardt et al. 2021a).

Priors for Aromatic Molecules in TMC-1 CP					
Component No.	v_{LSR} (km s ⁻¹)	Size (")	$\log_{10}(N_{\text{T}})$ (cm ⁻²)	T_{ex} (K)	ΔV (km s ⁻¹)
1	$\mathcal{N}(5.575, 0.01)$				
2	$\mathcal{N}(5.767, 0.01)$	$\mathcal{U}\{\text{min, max}\}$	$\mathcal{U}\{\text{min, max}\}$	$\mathcal{U}\{\text{min, max}\}$	$\mathcal{U}\{\text{min, max}\}$
3	$\mathcal{N}(5.892, 0.01)$				
4	$\mathcal{N}(6.018, 0.01)$				
Min	0.0				
Max	10.0	250	14.0	15.0	0.3
Priors for Aromatic Molecules in MC27/L1521F					
Component No.	v_{LSR} (km s ⁻¹)	Size (")	$\log_{10}(N_{\text{T}})$ (cm ⁻²)	T_{ex} (K)	ΔV (km s ⁻¹)
1	$\mathcal{N}(6.341, 0.01)$	$\delta(400)$	$\mathcal{U}\{\text{min, max}\}$	$\mathcal{N}(4.91, 0.10)$	$\mathcal{N}(0.16, 0.04)$
2	$\mathcal{N}(6.618, 0.01)$				
Min	0.0		10.0	1.0	0.1
Max	10.0		15.0	9.0	0.4

Table A2. Summary statistics of the marginalized posterior probability distributions from the MCMC analysis for phenalene in TMC-1. Priors used are reported in Table A1. The uncertainties are represented by the 16th and 84th percentile, also known as the 68% confidence interval, which corresponds to 1σ for a Gaussian distribution. The total column density and its uncertainty are derived by marginalizing over the posterior distributions for the column densities of each individual component and reporting the 50th, 16th, and 84th percentiles.

Phenalene (C ₁₃ H ₁₀) in TMC-1 CP					
Component No.	v_{LSR} (km s ⁻¹)	Size (")	N_{T} (10 ¹² cm ⁻²)	T_{ex} (K)	ΔV (km s ⁻¹)
1	5.575 ^{+0.010} _{-0.010}	128 ⁺⁸² ₋₈₄	0.44 ^{+1.37} _{-0.43}	9.91 ^{+1.73} _{-1.33}	0.254 ^{+0.024} _{-0.020}
2	5.754 ^{+0.009} _{-0.009}	153 ⁺⁶³ ₋₆₈	7.77 ^{+1.20} _{-0.98}		
3	5.892 ^{+0.010} _{-0.010}	118 ⁺⁸⁸ ₋₈₉	0.02 ^{+0.23} _{-0.02}		
4	6.036 ^{+0.009} _{-0.009}	123 ⁺⁸² ₋₆₈	7.08 ^{+1.97} _{-0.93}		
$N_{\text{T}}(\text{Total}): 1.53^{+0.27}_{-0.14} \times 10^{13} \text{ cm}^{-2}$					

(T. B. Adler et al. 2007; D. G. Liakos et al. 2013), with the correlation consistent double zeta basis set refined for F12 approaches cc-pVDZ-F12 (T. H. Dunning 1989; R. A. Kendall et al. 1992; E. R. Davidson 1996) orbital

basis set and the aug-cc-pVTZ/c (T. H. Dunning 1989; R. A. Kendall et al. 1992; F. Weigend et al. 2002; C. Hattig 2005) and cc-pVDZ-F12-CABS (K. A. Peterson et al. 2008; J. Noga & J. Simunek 2009; E. F. Valeev

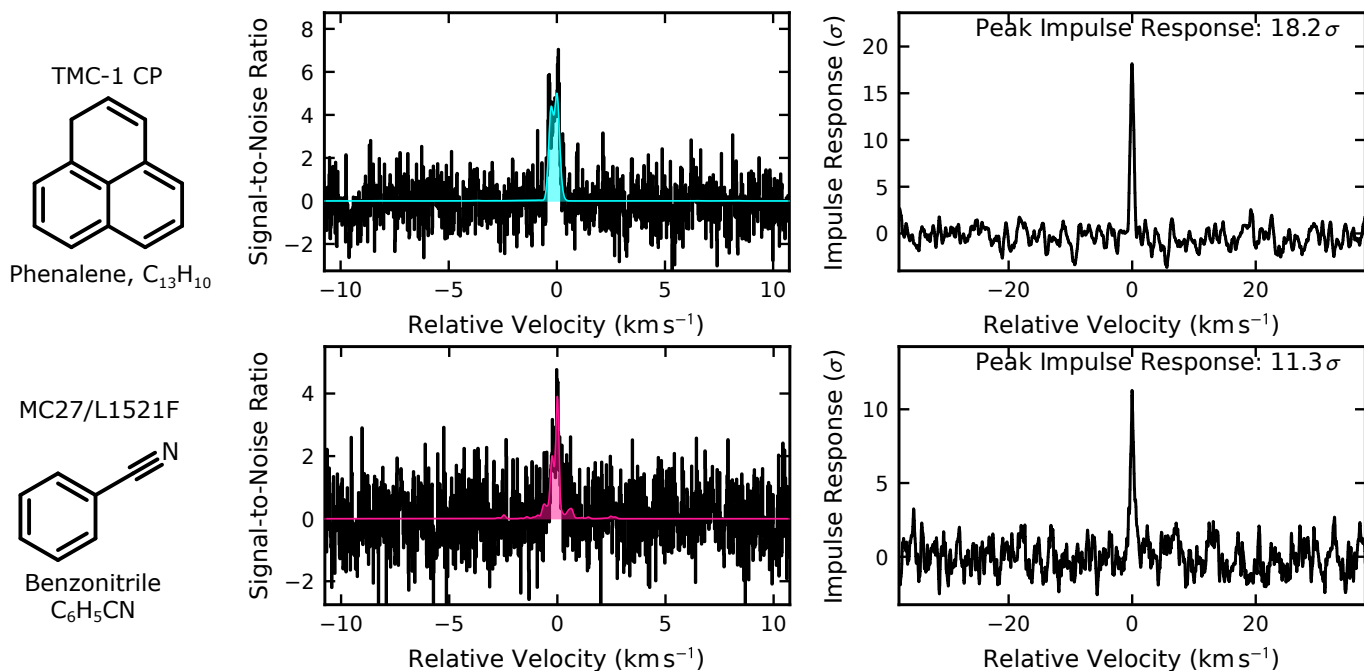


Figure A1. (Top left) Velocity-stacked spectra of the simulated phenalene emission (aqua) and observational data (black) and (top right) matched filter response of phenalene in the GOTHAM data toward TMC-1 CP. (Bottom left) Velocity-stacked spectra of the simulated benzonitrile emission (magenta) and observational data (black) and (bottom right) matched filter response of benzonitrile in the ARKHAM data toward MC27/L1521F. All plots were generated using the methodologies outlined in R. A. Loomis et al. (2021).

Table A3. Same as Table A2 for benzonitrile and phenalene in MC27/L1521F.

Benzonitrile (C_6H_5CN) in MC27/L1521F					
Component No.	v_{LSR} ($km\ s^{-1}$)	Size ($''$)	N_T ($10^{11}\ cm^{-2}$)	T_{ex} (K)	ΔV ($km\ s^{-1}$)
1	$6.343^{+0.009}_{-0.009}$	[400]	$2.85^{+0.42}_{-0.41}$	$4.91^{+0.08}_{-0.08}$	$0.156^{+0.041}_{-0.026}$
2	$6.617^{+0.011}_{-0.011}$	[400]	$0.81^{+0.37}_{-0.42}$		
$N_T(\text{Total}): 3.66^{+0.56}_{-0.58} \times 10^{11}\ cm^{-2}$					
Phenalene ($C_{13}H_{10}$) in MC27/L1521F					
Component No.	v_{LSR} ($km\ s^{-1}$)	Size ($''$)	N_T ($10^{13}\ cm^{-2}$)	T_{ex} (K)	ΔV ($km\ s^{-1}$)
1	$6.348^{+0.011}_{-0.011}$	[400]	$1.44^{+0.36}_{-0.35}$	$4.91^{+0.08}_{-0.08}$	$0.188^{+0.029}_{-0.028}$
2	$6.618^{+0.012}_{-0.012}$	[400]	$0.03^{+0.34}_{-0.03}$		
$N_T(\text{Total}): 1.47^{+0.49}_{-0.35} \times 10^{13}\ cm^{-2}$					

2004) auxiliary basis sets. All calculations were performed with ORCA 6.1.0 (F. Neese 2000, 2012, 2023, 2025).

A complete characterization of the reaction of CN with phenalene is beyond the scope of this work due to the large number of sites. However, an analysis of the initial addition of CN to phenalene and the subsequent prompt

elimination of an H atom from the carbon to which CN binds or from the CH_2 group was carried out. The addition of CN to the aromatic ring positions bearing a single H atom were all found to occur barrierlessly. The subsequent H atom elimination barriers, that result in a peri position sp^3 carbon, are found to be very submerged (-45 – $70\ kJ\ mol^{-1}$). Therefore, formation of 2-,

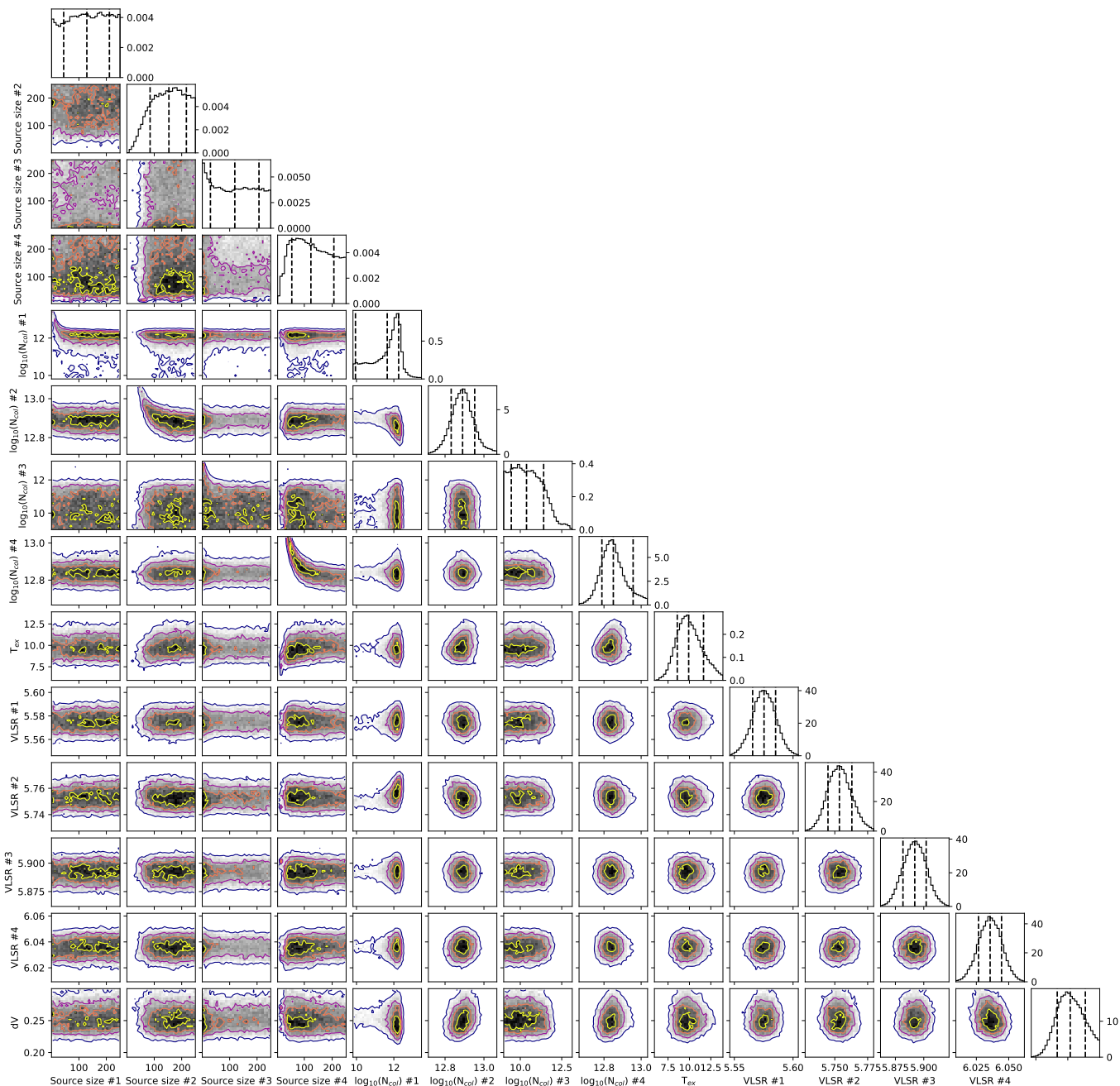


Figure A2. Parameter covariances and marginalized posterior distributions for the MCMC fit of phenalene in TMC-1 CP. 16th, 50th, and 84th confidence intervals (corresponding to $\pm 1\sigma$ for a Gaussian posterior distribution) are depicted as vertical lines on the diagonal plots.

3-, 4-, 5-, 6-, 7-, 8-cyano-1H-phenalene from their respective adducts is expected to be open at low temperatures. The barriers for H elimination yielding a non-peri sp^3 carbon were substantially emerged ($>+85$ kJ mol⁻¹) with a very endothermic product ($+160$ kJ mol⁻¹). As a result, 2-cyano-2H-phenalene is not predicted to form at low temperatures; whereas, 1-cyano-1H-phenalene can form following addition at the 3, 4, 6, 7, and 9 positions

(see Figures C4 and C5 for example structures and potential energy surface, respectively).

C.2. Prediction of site-specific rate coefficients

The rate coefficient for the reactions of CN with phenalene and indene were estimated with classical capture theory (Y. Georgievskii & S. J. Klippenstein 2005; N. A. West et al. 2019) in the manner applied in (G. Wenzel et al. 2025a,b; D. A. Stewart et al. 2025;

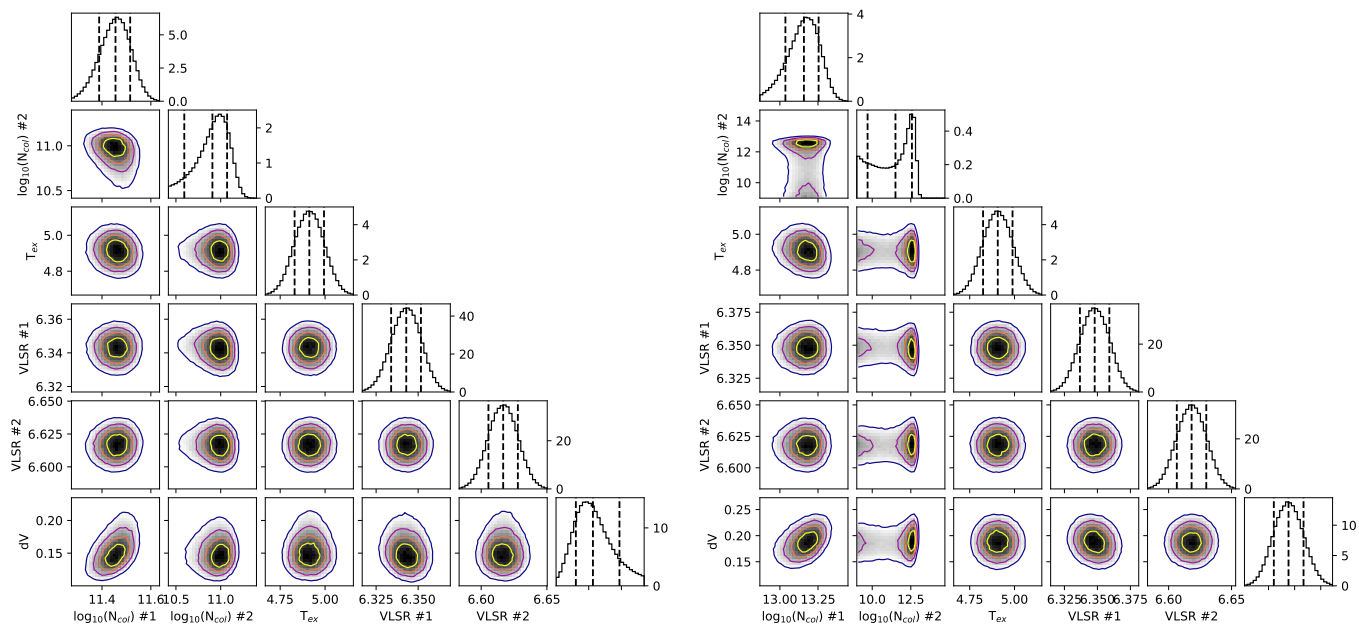


Figure A3. Parameter covariances and marginalized posterior distributions for the MCMC fits of benzonitrile (left) and phenalene (right) in MC27/L1521F. 16th, 50th, and 84th confidence intervals (corresponding to $\pm 1\sigma$ for a Gaussian posterior distribution) are depicted as vertical lines on the diagonal plots.

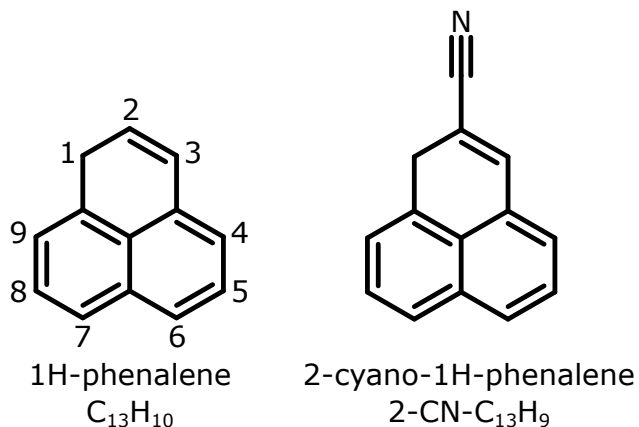


Figure C4. Structures of 1H-phenalene with its potential **substitution** sites and 2-cyano-1H-phenalene, as an example of one of the potential CN + phenalene products after H atom elimination.

R. H. J. Willis et al. 2026). With ionization energies, polarizabilities and dipole moments from the Computational Chemistry Comparison and Benchmark DataBase (R. I. Johnson 2022), NIST chemistry webbook (P. Linstrom & W. Mallard 2024), or calculated with ω B97M-D4/ma-def2-TZVPP. At 10 K, this predicts $k_{CN+phen} = 5.38^{+5.38}_{-2.69} \times 10^{-10} \text{ cm}^3\text{s}^{-1}$ and $k_{CN+ind} = 4.88^{+4.88}_{-2.44} \times 10^{-10} \text{ cm}^3\text{s}^{-1}$ for CN with phenalene and indene, respectively.

In the absence of an in-depth calculation of the long-range partitioning of the reactant flux into the adducts,

it is pragmatic to treat the site specificity statistically. This approach predicts the observed ratio of 1-, 2-, and 4-cyanopyrene (G. Wenzel et al. 2024, 2025a) in TMC-1 CP, and is within a factor of two for 1-, 3-, 4-, and 5-cyanoacenaphthylene (J. Cernicharo et al. 2024, 2026). If the initial attack yields prompt elimination of the H bound to the same carbon (which occurs via the lowest barriers in Table C5), this results in the formation of 2-, 3-, 4-, 5-, 6-, 7-, 8-, and 9-cyano-1H-phenalene in equal abundances with a rate coefficient of $k_{2-9} = 6.73^{+6.73}_{-3.36} \times 10^{-11} \text{ cm}^3\text{s}^{-1}$ at 10 K. If all submerged H elimination channels are equally competitive, 1-cyano-1H-phenalene will be the dominant product with $k_1 = 2.24^{+2.24}_{-1.12} \times 10^{-10} \text{ cm}^3\text{s}^{-1}$, 2-, 5-, 8-cyano-1H-phenalene formation is unchanged with $k_{2,5,8} = 6.73^{+6.73}_{-3.36} \times 10^{-11} \text{ cm}^3\text{s}^{-1}$ and 3-, 4-, 6-, 7-, 9-cyano-1H-phenalene formation is suppressed with $k_{3,4,6,7,9} = 2.24^{+2.24}_{-1.12} \times 10^{-11} \text{ cm}^3\text{s}^{-1}$.

C.3. Estimation of the abundance of different isomers of cyanophenalene in TMC-1

The astrochemical modeling in G. Wenzel et al. (2025a) derived the ratio of cyano-tagged benzene and indene from both the chemical age and the CN + aromatic rate coefficient. Here, the ratios predicted at 2×10^5 years are used in combination with the rate coefficients above, to predict the abundances of the CN tagged species from their bare PAH parents with the results summarized in Table C6. There is a reasonable agreement between the predicted and observed col-

Table B4. Column densities of molecular hydrogen and carbon-bearing cycles observed in TMC-1 CP and MC27/L1521F as presented in Fig. 2.

Molecules in TMC-1 CP				
Molecule	Chemical Formula	N_C	Column Density (10^{12} cm^{-2})	Reference
Molecular hydrogen	H_2	0	1.82×10^{10}	A. Fuente et al. (2019); J. M. Kirk et al. (2024)
Benzonitrile	$\text{C}_6\text{H}_5\text{CN}$	7	$1.65^{+0.09}_{-0.06}$	C. Xue et al. (2025)
1H-indene	C_9H_8	9	$11.4^{+3.7}_{-2.2}$	C. Xue et al. (2025)
2-cyanoindene	$2\text{-C}_9\text{H}_7\text{CN}$	10	$0.15^{+0.08}_{-0.03}$	C. Xue et al. (2025)
1H-cyclopent[cd]indene	C_{11}H_8	11	$6.0^{+0.5}_{-0.5}$	R. Fuentetaja et al. (2026)
1-cyanonaphthalene	$1\text{-C}_{10}\text{H}_7\text{CN}$	11	$0.80^{+0.81}_{-0.16}$	C. Xue et al. (2025)
2-cyanonaphthalene	$2\text{-C}_{10}\text{H}_7\text{CN}$	11	$0.53^{+0.14}_{-0.05}$	C. Xue et al. (2025)
1-cyanoacenaphthylene	$1\text{-C}_{12}\text{H}_7\text{CN}$	13	$1.09^{+0.40}_{-0.18}$	C. Xue et al. (2025)
3-cyanoacenaphthylene	$3\text{-C}_{12}\text{H}_7\text{CN}$	13	$0.7^{+0.07}_{-0.09}$	J. Cernicharo et al. (2026)
4-cyanoacenaphthylene	$4\text{-C}_{12}\text{H}_7\text{CN}$	13	$0.5^{+0.06}_{-0.09}$	J. Cernicharo et al. (2026)
5-cyanoacenaphthylene	$5\text{-C}_{12}\text{H}_7\text{CN}$	13	$0.77^{+0.38}_{-0.12}$	C. Xue et al. (2025)
1H-phenalene	$\text{C}_{13}\text{H}_{10}$	13	$15.3^{+2.7}_{-1.4}$	This work
1-cyanopyrene	$1\text{-C}_{16}\text{H}_9\text{CN}$	17	$0.91^{+0.19}_{-0.08}$	C. Xue et al. (2025)
2-cyanopyrene	$2\text{-C}_{16}\text{H}_9\text{CN}$	17	$0.57^{+0.18}_{-0.08}$	C. Xue et al. (2025)
4-cyanopyrene	$4\text{-C}_{16}\text{H}_9\text{CN}$	17	$0.92^{+0.35}_{-0.14}$	C. Xue et al. (2025)
Cyanocoronene	$\text{C}_{24}\text{H}_{11}\text{CN}$	25	$2.69^{+0.26}_{-0.23}$	G. Wenzel et al. (2025b)

Molecules in MC27/L1521F				
Molecule	Chemical Formula	N_C	Column Density (10^{12} cm^{-2})	Reference
Molecular hydrogen	H_2	0	1.68×10^{10}	S. Chitsazzadeh (2014)
Benzonitrile	$\text{C}_6\text{H}_5\text{CN}$	7	$0.366^{+0.056}_{-0.058}$	This work
1H-phenalene	$\text{C}_{13}\text{H}_{10}$	13	$14.7^{+4.9}_{-3.5}$	This work

umn densities of 2-cyanoindene in TMC-1 CP, if equal formation of each isomer occurs. Under the same approach 1/8th of the reaction flux results in the formation of each of 2-, 3-, 4-, 5-, 6-, 7-, 8-, and 9-cyano-1H-phenalene (9-CN- C_{13}H_9) with an abundance in TMC-

1 CP of $N(\text{C}_{13}\text{H}_9\text{CN}) = 2.72^{+3.70}_{-1.49} \times 10^{11} \text{ cm}^{-2}$. However, if all submerged H elimination channels are equally competitive, this value could rise to $N(\text{C}_{13}\text{H}_9\text{CN}) = 9.07^{+12.34}_{-4.98} \times 10^{11} \text{ cm}^{-2}$ for 1-cyano-1H-phenalene (1-CN- C_{13}H_9).

REFERENCES

- Adler, T. B., Knizia, G., & Werner, H.-J. 2007, The Journal of Chemical Physics, 127, 221106, doi: [10.1063/1.2817618](https://doi.org/10.1063/1.2817618)
- Agúndez, M., & Cernicharo, J. 2026, ACS Earth and Space Chemistry, doi: [10.1021/acsearthspacechem.6c00026](https://doi.org/10.1021/acsearthspacechem.6c00026)
- Agúndez, M., Marcelino, N., Tercero, B., & Cernicharo, J. 2023, Astronomy & Astrophysics, 677, L13, doi: [10.1051/0004-6361/202347524](https://doi.org/10.1051/0004-6361/202347524)
- Allamandola, L. J., Tielens, A. G. G. M., & Barker, J. R. 1985, The Astrophysical Journal, 290, L25, doi: [10.1086/184435](https://doi.org/10.1086/184435)
- Bergin, E., Calvet, N., D’Alessio, P., & Herczeg, G. J. 2003, The Astrophysical Journal, 591, L159, doi: [10.1086/377148](https://doi.org/10.1086/377148)
- Bourke, T. L., Myers, P. C., Ii, N. J. E., et al. 2006, The Astrophysical Journal, 649, L37, doi: [10.1086/508161](https://doi.org/10.1086/508161)
- Bull, J. N., Subramani, A., Liu, C., et al. 2025, Physical Review Letters, 134, 228002, doi: [10.1103/PhysRevLett.134.228002](https://doi.org/10.1103/PhysRevLett.134.228002)
- Burkhardt, A. M., Loomis, R. A., Shingledecker, C. N., et al. 2021a, Nature Astronomy, 5, 181, doi: [10.1038/s41550-020-01253-4](https://doi.org/10.1038/s41550-020-01253-4)

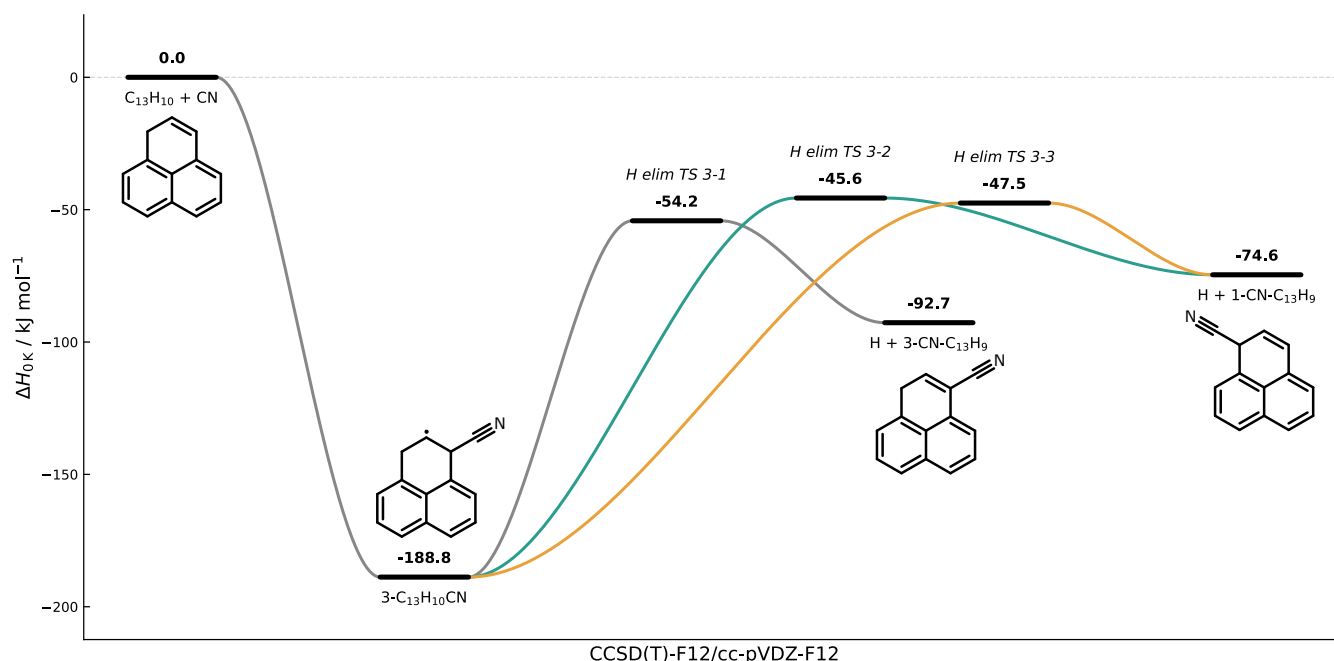


Figure C5. A subset of the potential energy surface for the addition of CN to phenalene and subsequent H atom elimination channels at the CCSD(T)-F12/cc-pVDZ-F12// ω B97M-D4/ma-def2-TZVPP level of theory. Only pathways upon addition to the 3-position (see Figure C4) are shown as an example. Other cyano-1H-phenalenes will form analogously and involving energies presented in Table C5.

Burkhardt, A. M., Lee, K. L. K., Changala, P. B., et al. 2021b, *The Astrophysical Journal Letters*, 913, L18, doi: [10.3847/2041-8213/abfd3a](https://doi.org/10.3847/2041-8213/abfd3a)

Cabezas, C., Agúndez, M., Pérez, C., et al. 2025, *Astronomy & Astrophysics*, 701, L8, doi: [10.1051/0004-6361/202556687](https://doi.org/10.1051/0004-6361/202556687)

Caldeweyher, E., Ehlert, S., Hansen, A., et al. 2019, *The Journal of Chemical Physics*, 150, 154122, doi: [10.1063/1.5090222](https://doi.org/10.1063/1.5090222)

Caldeweyher, E., Mewes, J.-M., Ehlert, S., & Grimme, S. 2020, *Physical Chemistry Chemical Physics*, 22, 8499, doi: [10.1039/D0CP00502A](https://doi.org/10.1039/D0CP00502A)

Cernicharo, J., Agúndez, M., Cabezas, C., et al. 2021a, *Astronomy and astrophysics*, 649, L15, doi: [10.1051/0004-6361/202141156](https://doi.org/10.1051/0004-6361/202141156)

Cernicharo, J., Agúndez, M., Kaiser, R. I., et al. 2021b, *Astronomy & Astrophysics*, 652, L9, doi: [10.1051/0004-6361/202141660](https://doi.org/10.1051/0004-6361/202141660)

Cernicharo, J., Cabezas, C., Fuentetaja, R., et al. 2024, *Astronomy & Astrophysics*, 690, L13, doi: [10.1051/0004-6361/202452196](https://doi.org/10.1051/0004-6361/202452196)

Cernicharo, J., Tercero, B., Marcelino, N., et al. 2026, *Astronomy & Astrophysics*, 705, L7, doi: [10.1051/0004-6361/202557893](https://doi.org/10.1051/0004-6361/202557893)

Chai, J.-D., & Head-Gordon, M. 2008, *The Journal of Chemical Physics*, 128, 084106, doi: [10.1063/1.2834918](https://doi.org/10.1063/1.2834918)

Chitsazzadeh, S. 2014, Ph.D. thesis. <https://ui.adsabs.harvard.edu/abs/2014PhDT.....423C>

Cooke, I. R., Gupta, D., Messinger, J. P., & Sims, I. R. 2020, *The Astrophysical Journal Letters*, 891, L41, doi: [10.3847/2041-8213/ab7a9c](https://doi.org/10.3847/2041-8213/ab7a9c)

Crapsi, A., Caselli, P., Walmsley, C. M., et al. 2004, *Astronomy & Astrophysics*, 420, 957, doi: [10.1051/0004-6361:20035915](https://doi.org/10.1051/0004-6361:20035915)

Davidson, E. R. 1996, *Chemical Physics Letters*, 260, 514, doi: [10.1016/0009-2614\(96\)00917-7](https://doi.org/10.1016/0009-2614(96)00917-7)

Debes, D. B., Mendes, M., Rodrigues, R., et al. 2025, *Astronomy & Astrophysics*, 693, A304, doi: [10.1051/0004-6361/202449818](https://doi.org/10.1051/0004-6361/202449818)

Dunning, Jr., T. H. 1989, *The Journal of Chemical Physics*, 90, 1007, doi: [10.1063/1.456153](https://doi.org/10.1063/1.456153)

Endres, C. P., Schlemmer, S., Schilke, P., Stutzki, J., & Müller, H. S. P. 2016, *Journal of Molecular Spectroscopy*, 327, 95, doi: [10.1016/j.jms.2016.03.005](https://doi.org/10.1016/j.jms.2016.03.005)

Favre, C., Vastel, C., Jimenez-Serra, I., et al. 2020, *Astronomy & Astrophysics*, 635, A189, doi: [10.1051/0004-6361/201937297](https://doi.org/10.1051/0004-6361/201937297)

Table C5. Energetics of selected channels in the reaction of CN and phenalene. DFT refers to ω B97M-D4/ma-def2-TZVPP, zpe scaled harmonic zero point energies, and CCSD(T)-F12 the CCSD(T)-F12/cc-pVDZ-F12 single point energies. ΔH_{0K} are the relative energies including ZPEs.

Structures	DFT energy	Energies / Ha		ΔH_{0K} /kJ mol ⁻¹	
		zpe	CCSD(T)-F12	DFT	CCSD(T)-F12
C ₁₃ H ₁₀ +CN	-594.5320723	0.190091178	-593.1626747	0.0	0.0
2-C ₁₃ H ₁₀ CN	-594.6433633	0.193911581	-593.2628278	-282.2	-252.9
H elim TS 2-1	-594.5653908	0.185834259	-593.1844863	-98.7	-68.4
H+2-CN-C ₁₃ H ₉	-594.5718148	0.184152848	-593.1935108	-119.9	-96.6
3-C ₁₃ H ₁₀ CN	-594.6194126	0.193201534	-593.2376985	-221.1	-188.8
H elim TS 3-1	-594.5599551	0.185602329	-593.1788335	-85.0	-54.2
H+3-CN-C ₁₃ H ₉	-594.5703500	0.18405476	-593.1919636	-116.3	-92.7
4-C ₁₃ H ₁₀ CN	-594.6220649	0.192895701	-593.2414129	-228.9	-199.4
H elim TS 4-1	-594.5616031	0.185630533	-593.1808713	-89.2	-59.5
H+4-CN-C ₁₃ H ₉	-594.5715500	0.184017725	-593.1930133	-119.6	-95.6
5-C ₁₃ H ₁₀ CN	-594.6128503	0.192859458	-593.2338463	-204.8	-179.6
H elim TS 5-1	-594.5578435	0.185546596	-593.1774470	-79.6	-50.7
H+5-CN-C ₁₃ H ₉	-594.5701196	0.183924273	-593.1917687	-116.1	-92.6
6-C ₁₃ H ₁₀ CN	-594.6298568	0.193166406	-593.2496779	-248.7	-220.4
H elim TS 6-1	-594.5624101	0.185623795	-593.1816438	-91.4	-61.5
H+6-CN-C ₁₃ H ₉	-594.5716307	0.184062593	-593.193162	-119.7	-95.9
7-C ₁₃ H ₁₀ CN	-594.6220803	0.19287403	-593.2414155	-229.0	-199.4
H elim TS 7-1	-594.5612959	0.185646406	-593.1801322	-88.4	-57.5
H+7-CN-C ₁₃ H ₉	-594.5714207	0.18403922	-593.1929296	-119.2	-95.3
8-C ₁₃ H ₁₀ CN	-594.6093772	0.192575678	-593.2294700	-196.4	-168.9
H elim TS 8-1	-594.5572414	0.185547271	-593.1763881	-78.0	-47.9
H+8-CN-C ₁₃ H ₉	-594.5701030	0.183922023	-593.1917136	-116.0	-92.4
9-C ₁₃ H ₁₀ CN	-594.6183946	0.192914712	-593.2388733	-219.2	-192.6
H elim TS 9-1	-594.5625299	0.185669984	-593.1815516	-91.6	-61.2
H+9-CN-C ₁₃ H ₉	-594.5726246	0.183988152	-593.1940215	-122.5	-98.3
H elimination from CH ₂ group in adducts 3,4,6,7,9					
H elim TS 3-2	-594.5565493	0.185691587	-593.1756352	-75.8	-45.6
H elim TS 3-3	-594.5572444	0.185578937	-593.1762520	-77.9	-47.5
H elim TS 4-2	-594.5574507	0.185671372	-593.1766367	-78.2	-48.3
H elim TS 4-3	-594.557819	0.185666238	-593.1769520	-79.2	-49.1
H elim TS 6-2	-594.558355	0.185599024	-593.1778964	-80.8	-51.8
H elim TS 6-3	-594.5585252	0.185597362	-593.1780215	-81.3	-52.1
H elim TS 7-2	-594.5578791	0.185647129	-593.1774521	-79.4	-50.5
H elim TS 7-3	-594.558122	0.185639032	-593.1776427	-80.1	-51.0
H elim TS 9-2	-594.5565115	0.185727614	-593.17615881	-75.6	-46.9
H elim TS 9-3	-594.5586103	0.185658865	-593.1780109	-81.3	-51.9
H + 1-CN-C ₁₃ H ₉	-594.5634837	0.184260979	-593.1852394	-97.8	-74.6

Frenklach, M., Clary, D. W., Gardiner, W. C., & Stein, S. E. 1985, Symposium (International) on Combustion, 20, 887, doi: [10.1016/S0082-0784\(85\)80578-6](https://doi.org/10.1016/S0082-0784(85)80578-6)

Frenklach, M., Jasper, A. W., & Mebel, A. M. 2024, Physical Chemistry Chemical Physics, doi: [10.1039/D4CP00096J](https://doi.org/10.1039/D4CP00096J)

Fuente, A., Navarro, D. G., Caselli, P., et al. 2019, Astronomy & Astrophysics, 624, A105, doi: [10.1051/0004-6361/201834654](https://doi.org/10.1051/0004-6361/201834654)

Fuentetaja, R., Cabezas, C., Agúndez, M., et al. 2026, Astronomy & Astrophysics, 706, L10, doi: [10.1051/0004-6361/202558398](https://doi.org/10.1051/0004-6361/202558398)

Table C6. Observed (obs) and predicted (pred) parent to child ratios (H/CN) for cyano functionalized indene and phenalene isomers in TMC-1 CP. Observed column densities are taken from recent observations of TMC-1 CP; from this work (1) and from C. Xue et al. (2025) (2). The site-specific scenario refers to 1/6th and 1/8th of flux per isomer, For CN + indene and CN + phenalene, respectively.

	Phenalene (1)	Indene (2)
$N(\text{H})$ (10^{13} cm^{-2})	$1.53^{+0.27}_{-0.14}$	$1.14^{+0.37}_{-0.22}$
$N(\text{CN})_{\text{obs}}$ (10^{11} cm^{-2})	—	$1.50^{+0.80}_{-0.30}$
$[\text{H}/\text{CN}]_{\text{obs}}$	—	76^{+49}_{-36}
Total $[\text{H}/\text{CN}]_{\text{pred}}$	$7.03^{+7.12}_{-3.52}$	$7.75^{+7.86}_{-3.89}$
Site specific $[\text{H}/\text{CN}]_{\text{pred}}$	$56.2^{+57.0}_{-28.2}$	$46.5^{+47.2}_{-23.3}$
Total $N(\text{CN})_{\text{pred}}$ (10^{12} cm^{-2})	$2.18^{+2.96}_{-1.19}$	$1.47^{+2.44}_{-0.88}$
Site specific $N(\text{CN})_{\text{pred}}$ (10^{11} cm^{-2})	$2.72^{+3.70}_{-1.49}$	$2.45^{+4.07}_{-1.47}$

- Georgievskii, Y., & Klippenstein, S. J. 2005, *The Journal of Chemical Physics*, 122, 194103, doi: [10.1063/1.1899603](https://doi.org/10.1063/1.1899603)
- Hanwell, M. D., Curtis, D. E., Lonie, D. C., et al. 2012, *Journal of Cheminformatics*, 4, 17, doi: [10.1186/1758-2946-4-17](https://doi.org/10.1186/1758-2946-4-17)
- Hattig, C. 2005, *Physical Chemistry Chemical Physics*, 7, 59, doi: [10.1039/B415208E](https://doi.org/10.1039/B415208E)
- Ishida, K., Morokuma, K., & Komornicki, A. 1977, *The Journal of Chemical Physics*, 66, 2153, doi: [10.1063/1.434152](https://doi.org/10.1063/1.434152)
- Johansson, K. O., Head-Gordon, M. P., Schrader, P. E., Wilson, K. R., & Michelsen, H. A. 2018, *Science*, 361, 997, doi: [10.1126/science.aat3417](https://doi.org/10.1126/science.aat3417)
- Johnson, R. I. 2022, NIST computational chemistry comparison and benchmark database, <http://cccbdb.nist.gov/>
- Kamer, J., Schleier, D., Donker, M., et al. 2023, *Physical Chemistry Chemical Physics*, 25, 29070, doi: [10.1039/D3CP03977C](https://doi.org/10.1039/D3CP03977C)
- Kauffmann, J., Bertoldi, F., Evans II, N. J., & c2d Collaboration, T. 2005, *Astronomische Nachrichten*, 326, 878, doi: <https://doi.org/10.1002/asna.200510446>
- Kendall, R. A., Dunning, Jr., T. H., & Harrison, R. J. 1992, *The Journal of Chemical Physics*, 96, 6796, doi: [10.1063/1.462569](https://doi.org/10.1063/1.462569)
- Kesharwani, M. K., Brauer, B., & Martin, J. M. L. 2014, *The Journal of Physical Chemistry A*, 119, 1701, doi: [10.1021/jp508422u](https://doi.org/10.1021/jp508422u)
- Kirk, J. M., Ward-Thompson, D., Di Francesco, J., et al. 2024, *Monthly Notices of the Royal Astronomical Society*, 532, 4661, doi: [10.1093/mnras/stae1633](https://doi.org/10.1093/mnras/stae1633)
- Knizia, G., Adler, T. B., & Werner, H.-J. 2009, *The Journal of Chemical Physics*, 130, 054104, doi: [10.1063/1.3054300](https://doi.org/10.1063/1.3054300)
- Lehtola, S., Steigemann, C., Oliveira, M. J. T., & Marques, M. A. L. 2018, *SoftwareX*, 7, 1, doi: [10.1016/j.softx.2017.11.002](https://doi.org/10.1016/j.softx.2017.11.002)
- Levey, Z. D., Laws, B. A., Sundar, S. P., et al. 2022, *The Journal of Physical Chemistry A*, 126, 101, doi: [10.1021/acs.jpca.1c08310](https://doi.org/10.1021/acs.jpca.1c08310)
- Liakos, D. G., Izsák, R., Valeev, E. F., & Neese, F. 2013, *Molecular Physics*, 111, 2653, doi: [10.1080/00268976.2013.824624](https://doi.org/10.1080/00268976.2013.824624)
- Linstrom, P., & Mallard, W. 2024, NIST chemistry WebBook, NIST standard reference database number 69, <https://doi.org/10.18434/T4D303>
- Loomis, R. A., Shingledecker, C. N., Langston, G., et al. 2016, *Monthly Notices of the Royal Astronomical Society*, 463, 4175, doi: [10.1093/mnras/stw2302](https://doi.org/10.1093/mnras/stw2302)
- Loomis, R. A., Burkhardt, A. M., Shingledecker, C. N., et al. 2021, *Nature Astronomy*, 5, 188, doi: [10.1038/s41550-020-01261-4](https://doi.org/10.1038/s41550-020-01261-4)
- Léger, A., & Puget, J. L. 1984, *Astronomy & Astrophysics*, 500, 279
- Marciniak, A., Joblin, C., Mulas, G., Mundlapati, V. R., & Bonnamy, A. 2021, *Astronomy & Astrophysics*, 652, A42, doi: [10.1051/0004-6361/202140737](https://doi.org/10.1051/0004-6361/202140737)
- Mardirossian, N., & Head-Gordon, M. 2016, *The Journal of Chemical Physics*, 144, 214110, doi: [10.1063/1.4952647](https://doi.org/10.1063/1.4952647)
- McCarthy, M. C., & McGuire, B. A. 2026, doi: [10.1146/annurev-physchem-082324-010544](https://doi.org/10.1146/annurev-physchem-082324-010544)
- McGuire, B. A., Burkhardt, A. M., Kalenskii, S., et al. 2018, *Science*, 359, 202, doi: [10.1126/science.aao4890](https://doi.org/10.1126/science.aao4890)
- McGuire, B. A., Xue, C., Lee, K. L. K., El-Abd, S., & Loomis, R. A. 2024, molsim, Zenodo, doi: [10.5281/zenodo.12697227](https://doi.org/10.5281/zenodo.12697227)
- McGuire, B. A., Burkhardt, A. M., Loomis, R. A., et al. 2020, *The Astrophysical Journal Letters*, 900, L10, doi: [10.3847/2041-8213/aba632](https://doi.org/10.3847/2041-8213/aba632)
- McGuire, B. A., Loomis, R. A., Burkhardt, A. M., et al. 2021, *Science*, 371, 1265, doi: [10.1126/science.abb7535](https://doi.org/10.1126/science.abb7535)
- Neese, F. 2000, *Chemical Physics Letters*, 325, 93, doi: [10.1016/S0009-2614\(00\)00662-X](https://doi.org/10.1016/S0009-2614(00)00662-X)

- Neese, F. 2012, WIREs Computational Molecular Science, 2, 73, doi: [10.1002/wcms.81](https://doi.org/10.1002/wcms.81)
- Neese, F. 2023, Journal of Computational Chemistry, 44, 381, doi: [10.1002/jcc.26942](https://doi.org/10.1002/jcc.26942)
- Neese, F. 2025, WIREs Computational Molecular Science, 15, doi: [10.1002/wcms.70019](https://doi.org/10.1002/wcms.70019)
- Neese, F., Wennmohs, F., Becker, U., & Riplinger, C. 2020, The Journal of Chemical Physics, 152, 224108, doi: [10.1063/5.0004608](https://doi.org/10.1063/5.0004608)
- Noga, J., & Simunek, J. 2009, Chemical Physics, 356, 1, doi: [10.1016/j.chemphys.2008.10.012](https://doi.org/10.1016/j.chemphys.2008.10.012)
- O'Connor, G. D., Chan, B., Sanelli, J. A., et al. 2017, Chemical Science, 8, 1186, doi: [10.1039/C6SC03787A](https://doi.org/10.1039/C6SC03787A)
- O'Connor, G. D., Troy, T. P., Roberts, D. A., et al. 2011, Journal of the American Chemical Society, 133, 14554, doi: [10.1021/ja206322n](https://doi.org/10.1021/ja206322n)
- Peterson, K. A., Adler, T. B., & Werner, H.-J. 2008, The Journal of Chemical Physics, 128, 084102, doi: [10.1063/1.2831537](https://doi.org/10.1063/1.2831537)
- Porfrier, D. P., Azyazov, V. N., & Mebel, A. M. 2020, Combustion and Flame, 213, 302, doi: [10.1016/j.combustflame.2019.11.038](https://doi.org/10.1016/j.combustflame.2019.11.038)
- Rap, D. B., Schrauwen, J. G. M., Redlich, B., & Brünken, S. 2024, Physical Chemistry Chemical Physics, doi: [10.1039/D3CP05574D](https://doi.org/10.1039/D3CP05574D)
- Rauhut, G., Knizia, G., & Werner, H.-J. 2009, The Journal of Chemical Physics, 130, 054105, doi: [10.1063/1.3070236](https://doi.org/10.1063/1.3070236)
- Reizer, E., Viskolcz, B., & Fiser, B. 2022, Chemosphere, 291, 132793, doi: [10.1016/j.chemosphere.2021.132793](https://doi.org/10.1016/j.chemosphere.2021.132793)
- Rivilla, V. M., Andrés, D. S., Sanz-Novio, M., et al. 2026, Aromatic rings in the Central Molecular Zone: Benzonitrile, arXiv, doi: [10.48550/arXiv.2604.24510](https://doi.org/10.48550/arXiv.2604.24510)
- Schöller, L., Spezzano, S., Sipilä, O., et al. 2026, Tracing the sulfur depletion in starless and pre-stellar cores, arXiv, doi: [10.48550/arXiv.2605.13635](https://doi.org/10.48550/arXiv.2605.13635)
- Sita, M. L., Changala, P. B., Xue, C., et al. 2022, The Astrophysical Journal Letters, 938, L12, doi: [10.3847/2041-8213/ac92f4](https://doi.org/10.3847/2041-8213/ac92f4)
- Stewart, D. A., Speak, T. H., Yuan, E. Q. H., et al. 2025, The Journal of Physical Chemistry A, 129, 11400, doi: [10.1021/acs.jpca.5c05772](https://doi.org/10.1021/acs.jpca.5c05772)
- Stockett, M. H., Bull, J. N., Cederquist, H., et al. 2023, Nature Communications, 14, 395, doi: [10.1038/s41467-023-36092-0](https://doi.org/10.1038/s41467-023-36092-0)
- Subramani, A., Bull, J. N., Cederquist, H., et al. 2025, ACS Earth and Space Chemistry, doi: [10.1021/acsearthspacechem.5c00283](https://doi.org/10.1021/acsearthspacechem.5c00283)
- Tokuda, K., Omura, M., Harada, N., et al. 2026, The Astrophysical Journal Letters, 1001, L1, doi: [10.3847/2041-8213/ae47ec](https://doi.org/10.3847/2041-8213/ae47ec)
- Valeev, E. F. 2004, Chemical Physics Letters, 395, 190, doi: [10.1016/j.cplett.2004.07.061](https://doi.org/10.1016/j.cplett.2004.07.061)
- Weigend, F. 2006, Physical Chemistry Chemical Physics, 8, 1057, doi: [10.1039/B515623H](https://doi.org/10.1039/B515623H)
- Weigend, F., & Ahlrichs, R. 2005, Physical Chemistry Chemical Physics, 7, 3297, doi: [10.1039/B508541A](https://doi.org/10.1039/B508541A)
- Weigend, F., Kohn, A., & Hattig, C. 2002, The Journal of Chemical Physics, 116, 3175, doi: [10.1063/1.1445115](https://doi.org/10.1063/1.1445115)
- Wenzel, G., Cooke, I. R., Changala, P. B., et al. 2024, Science, 386, 810, doi: [10.1126/science.adq6391](https://doi.org/10.1126/science.adq6391)
- Wenzel, G., Speak, T. H., Changala, P. B., et al. 2025a, Nature Astronomy, 9, 262, doi: [10.1038/s41550-024-02410-9](https://doi.org/10.1038/s41550-024-02410-9)
- Wenzel, G., Gong, S., Xue, C., et al. 2025b, The Astrophysical Journal Letters, 984, L36, doi: [10.3847/2041-8213/adc911](https://doi.org/10.3847/2041-8213/adc911)
- West, N. A., Millar, T. J., de Sande, M. V., et al. 2019, The Astrophysical Journal, 885, 134, doi: [10.3847/1538-4357/ab480e](https://doi.org/10.3847/1538-4357/ab480e)
- Willis, R. H. J., Speak, T. H., Byrne, A. N., Shingledecker, C. N., & Cooke, I. R. 2026, arXiv preprint arXiv:2604.21892
- Xue, C. 2025, GOTHAM spectral pipeline, Zenodo, doi: [10.5281/zenodo.15678187](https://doi.org/10.5281/zenodo.15678187)
- Xue, C., Byrne, A. N., Morgan, L., et al. 2025, The Astrophysical Journal Supplement Series, 281, 9, doi: [10.3847/1538-4365/ae04e5](https://doi.org/10.3847/1538-4365/ae04e5)
- Yang, H., Herczeg, G. J., Linsky, J. L., et al. 2011, The Astrophysical Journal, 744, 121, doi: [10.1088/0004-637X/744/2/121](https://doi.org/10.1088/0004-637X/744/2/121)
- Zhao, L., Kaiser, R. I., Xu, B., et al. 2018, Nature Astronomy, 2, 413, doi: [10.1038/s41550-018-0399-y](https://doi.org/10.1038/s41550-018-0399-y)
- Zhao, L., Kaiser, R. I., Lu, W., et al. 2020, Physical Chemistry Chemical Physics, 22, 15381, doi: [10.1039/D0CP02216K](https://doi.org/10.1039/D0CP02216K)
- Zheng, J., Xu, X., & Truhlar, D. G. 2011, Theoretical Chemistry Accounts, 128, 295, doi: [10.1007/s00214-010-0846-z](https://doi.org/10.1007/s00214-010-0846-z)